Hindawi Publishing Corporation
Advances in Astronomy
Volume 2011, Article ID 508381, 13 pages
doi:10.1155/2011/508381

Research Article

Galaxy Evolution in a Pilot Survey up to $z = 1$ and CDM Halos

E. Giraud,[1] J. Melnick,[2] Q.-S. Gu,[3] H. Quintana,[4] F. Selman,[2] I. Toledo,[4] and P. Zelaya[4]

[1] *Laboratory of Theoretical Physics and Astroparticles, Montpellier University, 34095 Montpellier, France*
[2] *European Southern Observatory, Alonso de Córdova, Santiago, 3107, Chile*
[3] *Department of Astronomy, Nanjing University, Nanjing 210093, China*
[4] *Department of Astronomy and Astrophysics, P. Universidad Catolica de Chile, Casilla, Santiago, 306, Chile*

Correspondence should be addressed to E. Giraud, edmond.giraud@lpta.in2p3.fr

Received 8 June 2010; Accepted 15 July 2010

Academic Editor: Gary Wegner

We study spectral evolution of galaxies in a magnitude limited sample of 550 galaxies from $z = 1$ down to $z = 0.3$ on a pencil beam of $\approx 10' \times 10'$. We concentrate on the large apparent cosmological structures along the line of sight, and we bin our individual galaxy spectra to obtain representative high S/N spectra based upon these structures. We divide the resulting average spectra in three groups to facilitate the analysis:galaxies with pure absorption line spectra, galaxies with emission lines and blue continua, and galaxies with emission lines and red continua. We revisit the question of downsizing in emission-line galaxies between $z = 0.9$ and $z = 0.45$ in our pencil-beam and find the following results: strong star formation in emission line galaxies, aging in emission line galaxies, and aging in absorption systems, are shifting from bright to faint systems as cosmological time increases. Each redshift bin is repopulated in new starbursts. Therefore at redshifts $z \leqslant 1$ galaxy formation is downsizing both in luminosity and number density. Our observations indicate that at $z \leqslant 1$ star formation and hierarchical structure formation of CDM halos are not in phase.

1. Introduction

In the course of an investigation of the diffuse intergalactic light in X-ray emitting clusters at intermediate redshifts [1], we obtained redshifts and flux distributions for 654 galaxies of which 550 are in a pencil beam of $10' \times 10'$ and at $0.275 \leqslant z \leqslant 1.05$. In fact, our spectroscopy provides a 50–60% complete sample of galaxies uniformly down to $R = 23$. The vast majority of our individual spectra reduced to zero redshift have S/N ratios per 2.6 Å pixel larger than 3 at 4200 Å. Our pencil beam sample covers a redshift range up to $z = 1$ (with some galaxies up to $z = 1.7$). In standard cosmology with $H_o = 75\,\mathrm{km\,s^{-1}\,Mpc^{-1}}$, $\Omega_{0,m} = 0.30$, and $\Omega_{0,\Lambda} = 0.70$, this range provides a large leverage of about 3000 Mpc or 7 Gyr, which should be sufficient to extract some of the most conspicuous characteristics on galaxy evolution at $z \leqslant 1$. About half of all stars seem to be still forming, mostly in disks, in this range [2, 3].

Our sample compares in size with the DEEP1 spectroscopic pilot survey [4] but is far smaller than large surveys such as DEEP2, VVDS, and GOODS. The main advantage of a pilot survey is that it can be handled rather easily by a single (or a few) researcher(s) having multiple parameters in mind. It can be used to test new methods, new ideas, or to make independent control, which in a second step can be applied to large surveys, requiring much more manpower.

More than a decade ago, [5] suggested that while the most massive galaxies were formed early in the Universe, star formation is progressively shifted to smaller systems, the so-called downsizing effect. This effect had been confirmed by several later studies [6, 7]. The downsizing detected in samples of galaxies at different redshifts has been termed "downsizing in time" to be distinguished from the "archaeological downsizing" which refers to the observation that less massive early type galaxies formed their stellar populations later and over a longer time span than the more massive ones [8, 9].

Cold Dark Matter (CDM) models are hierarchical in the sense that large halos are built from the merging of small halos. Therefore, downsizing seems to be in conflict with hierarchical structure formation. In the present paper we revisit the question of downsizing, and we investigate the variation of star formation in emission-line galaxies with

Table 1: Properties of galaxies in the field of RX J0054.0-2823.

obj	RA (α) J2000	DEC (δ) J2000	z	m_R	V km/s	$V_{\rm err}$ km/s	R_T	Nobs	lines
23	13.598707	−28.434965	0.79304	22.78	237912	161	4.7	1	K–H
26	13.590379	−28.416917	0.77636	22.26	232908	77	8.1	1	[OII]–H10–H9–H

cosmological age, the aging in emission-line galaxies, and the aging in absorption systems.

The paper is structured as follows. Section 2 summarizes observations and the data reduction procedures. Section 3 presents observed variations in spectral energy distribution with redshift for absorption and emission systems, which are discussed with the use of population synthesis models. Section 4 is dedicated to population variations with z and luminosity in absorption systems. In Section 5 we partition emission-line galaxies in blue and red systems and study them separately. Down-sizing is in Section 5.4.

2. Observations and Data Reduction

The observations (ESO program 078A–0456(A)) were obtained with the FORS2 instrument [10] on the Cassegrain focus of the VLT UT1 telescope in multiobject spectroscopy mode with the exchangeable mask unit (MXU). We describe in joint paper [11] the details of the observations, data reductions and calibrations. The relative fluxes per wavelength of the calibrated spectra can be compared with stellar population models, in arbitrary unit.

The 4000 Å break amplitude definition used in the present paper is the "narrow" 4000 Å break defined by Balogh et al. [12] as the flux ratio in the range 4000–4100 Å over 3850–3950 Å (e.g., [13]). The error in D(4000) is calculated from the spectral noise in the two passbands. The equivalent widths of [OII] and of Hδ were measured by using the ESO-MIDAS (www.eso.org/projects/esomidas) subpackage ALICE which is dedicated to spectral analysis (rebinning, fluxes, continuum fitting, lines fitting, equivalent widths, flux in lines, ...). Full observational measurement errors on indexes of individual spectra were obtained by measuring D(4000) and EQW([OII]) on spectra with multiple observations. Thus 17% of the spectra have typical errors of 4% in D(4000) and 10% in EQW([OII]); 54% have typical errors of 8% in D(4000) and 20% in EQW([OII]); and 14% have poorer spectra with typical errors of 16% in D(4000) and 40% in EQW([OII]).

The ESO data of our program are presently in the public domain. The Catalog is available on request and will be made public by Centre des Données Stellaires in Strasbourg. It presents positions, redshifts, Petrossian R-magnitudes, and line identifications for the full sample of 654 galaxies observed in our program. The radial velocities and the corresponding measurement errors are also given. Table 1 is illustrative of the information contained in the full table.

Figure 1 shows the R-magnitude histogram of the galaxies with measured redshifts superimposed on the magnitude histogram of all galaxies in our pencilbeam indicating that

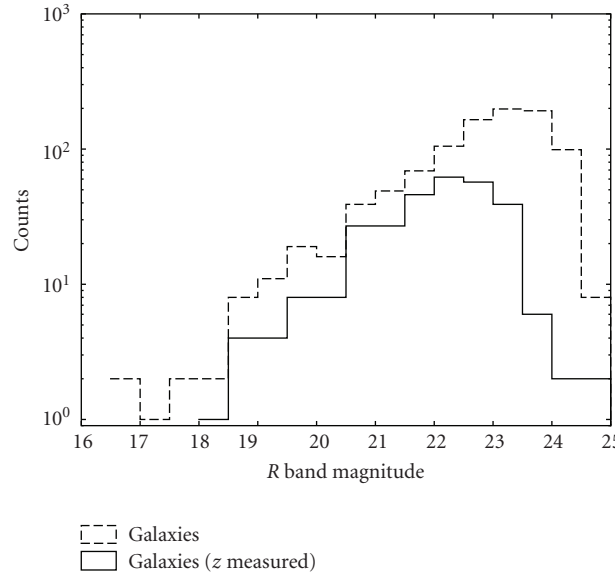

Figure 1: R-magnitude histogram of galaxies with measured redshift in the central beam.

our observations sample at a rate of 50–60% the population of galaxies in the magnitude bin $R = 20.5$–21.5 and at a rate 60–65% in the magnitude bin $R = 21.5$–22.5. The sampling seems fairly representative in the magnitude bin $R = 22.5$–23.0, and sparse at $R > 23$. The apparent increase in incompleteness toward brighter magnitudes is due to two selection bias in the following observations: (1) we tried to counterbalance Malmquist bias by observing the largest possible number of galaxies in the magnitude range $R = 22$–23 missing some objects in the bin $R = 20.5$–21.5, (2) our observations were designed to avoid bright galaxies at redshifts $z \leqslant 0.25$.

The R-band average magnitudes of galaxies in each redshift bin are given in Table 2 separately for absorption, "red" and "blue" emission-line galaxies, together with the adopted distance moduli. The partition "red" versus "blue" is defined by the median spectral slope in each redshift bin (Section 5.1).

We used the R-band photometry to calibrate individual spectra by convolving each spectrum with a box filter 1290 Å wide, centered at $\lambda = 6460$ Å. Once the spectra were calibrated in the observer R-band, we measured the average fluxes in the wavelength range 4150–4250 Å of the galaxies, which we normalized to the flux of blue emission galaxies at $\langle z \rangle = 0.9$ to compute the luminosity index f. Thus f (that is equal to 1 for blue galaxies at $\langle z \rangle = 0.9$) is an indicator of AB(4200) that allows us to compare the luminosities of

Table 2: Average R-band magnitudes of absorption systems (abs), and red and blue emission-line galaxies. The adopted distance moduli $(m-M)_0$ and the 4150–4250 Å fluxes f normalized to the blue galaxies at $z = 0.9$ are also tabulated.

$\langle z\rangle$	R(abs)	R(red)	R(blue)	$(m-M)_0$	f(abs)	f(red)	f(blue)
0.29	19.80	20.12	20.97	40.18	0.74	0.72	0.48
0.43	20.24	20.59	20.95	40.86	1.08	0.92	0.75
0.65	21.50	21.60	21.94	41.51	1.42	1.28	0.86
0.9	22.45	22.13	22.35	41.98	2.08	1.70	1

red and blue galaxies at a given redshift and to investigate luminosity variations with z.

Figure 2 presents the magnitude redshift relation and the cone diagrams for the full sample. The points are color coded according to the presence or absence of emission-lines.

A cursory inspection of Figure 2 reveals the presence of several conspicuous structures walls of objects spanning almost the entire field of view over the full range of redshifts covered by our observations. Making bins centered on the peaks of the redshift distribution maximizes the number of objects in each bin and minimizes its redshift dispersion. So using the apparent structures rather than a blind slicing appears well adapted to our sample.

3. Evolution in the Pencil Beam: Number-Weighted Analysis of Combined Spectral Types

Each galaxy spectrum was wavelength calibrated, corrected for instrument response, rebinned to zero redshift, and normalized to have the same flux in the wavelength range $\Delta\lambda = 4050$–4250 Å.

The normalization gives more weight to the more numerous galaxies than to the few very luminous ones, and is adapted to extract spectral properties from bright high-z galaxies to fainter low-z objects. In particular, downsizing, where the bulk of star formation shifts from bright to faint galaxies [6, 14], requires to compare bright and faint systems using the same weight.

The redshift range of our pencil beam survey goes up to $z = 1.72$ with a strong decline above $z \sim 1$. We have truncated the sample at $z = 1.05$ and assembled the spectra in bins centered on (pseudo) structures at 0.29, 0.41, 0.45, 0.63, 0.68, 0.82, and 0.99 to build high S/N composite spectra for each bin. In order to compensate (or at least alleviate) for Malmquist bias we rejected objects fainter than $M_R = -18.8$ mostly at $z \leqslant 0.45$ (Figure 2(a)). A sample completely free of Malmquist bias would require a cutoff at $M_R \sim -20.5$. For clarity of the figures throughout the paper, we often combined the mean spectra at $z = 0.41$ and 0.45 into a single bin at $\langle z\rangle = 0.43$, the spectra at $z = 0.63$ and 0.68 into a bin at $\langle z\rangle = 0.65$, and in some cases the spectra at $z = 0.82$ and 0.99 into a bin at $\langle z\rangle = 0.9$. The spectra of all galaxies in these five combined redshift bins are shown in Figure 3, where we show the spectra of absorption systems (a), and emission-line galaxies (b), separately. The S/N ratios of the combined spectra, measured in the wavelength range 4150–4250 Å to avoid prominent lines, are given in the relevant tables and/or in the figure captions.

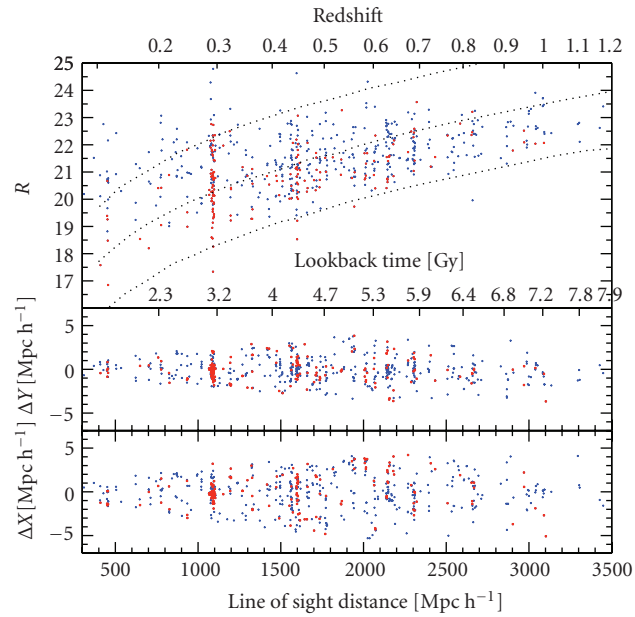

Figure 2: (a) Magnitude redshift relation for the full sample. The three lines overploted over the measured points correspond to absolute R magnitudes of -22.5, -20.5, and -18.5. The distances have been calculated using a cosmology with $\Omega_{0,\Lambda} = 0.70$, $\Omega_{0,m} = 0.30$, $w = -1$, and $H_0 = 75\,\mathrm{km\,s^{-1}\,Mpc^{-1}}$ ($h = H_0/75\,\mathrm{km\,s^{-1}\,Mpc^{-1}}$). Red dots are galaxies with no emission-lines and blue dots are galaxies with emission-lines. (b) Cone diagrams in Dec for all the galaxies measured in the field of RX J0054.0-2823. The scales is in Mpc calculated using the angular distance for the standard cosmology. The detection threshold for emission-lines is EQW([OII]) ~ 2-3 Å. (c) Same as (b) but for RA.

The most conspicuous spectral change with redshift is a decrease in flux redward of the G-band from $\langle z\rangle = 0.29$ and $\langle z\rangle = 0.43$ to higher z coupled to an increase to the blue of [OII] from $\langle z\rangle = 0.65$ to $\langle z\rangle = 0.82$ and higher z. Since we normalized the spectra at $\lambda\lambda 4050 - 4250$ Å, this redistribution of flux is manifested as a rotation of the continuum around a pivot point at $\lambda \sim 4150$ Å. This rotation of the normalized spectra implies a systematic change in the galaxy populations entering the sample with redshift: more star forming galaxies at higher z, and more galaxies with old stars at lower z. This is quantified in Table 3 that shows that the redshift dependence of the 4000 Å break amplitude is more substantial in emission-lines galaxies, while the

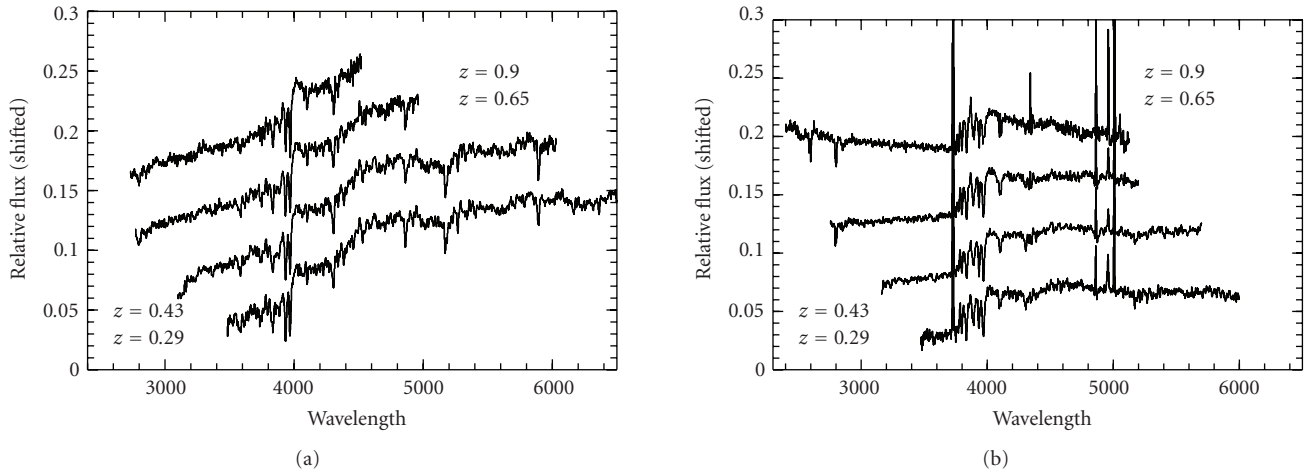

Figure 3: Composite spectra of absorption systems (a); and emission-line galaxies (b) normalized in the wavelength range $\Delta\lambda$ = 4050–4250 Å. All individual galaxies are brighter than $M_R = -18.8$.

Table 3: 4000 Å break amplitudes for absorption (abss), and emission (em) galaxies and equivalent width of Hδ for absorption galaxies. The errors are those in the index measurements. The S/N ratios are those of the combined spectra measured in the wavelength range 4050–4250 Å. The magnitude cutoff is $M_R = -18.8$ for all the redshift bins, but is affected by Malmquist bias.

	Absorption systems			Emission systems	
$\langle z \rangle$	D(4000)	EQW(Hδ)	S/N	D(4000)	S/N
0.29	1.67 ± 0.065	−1.5 ± 0.2	23	1.22 ± 0.02	32
0.43	1.70 ± 0.06	−1.5 ± 0.2	22	1.22 ± 0.01	52
0.65	1.60 ± 0.055	−1.8 ± 0.2	24	1.14 ± 0.01	35
0.82	1.57 ± 0.06	−2.4 ± 0.5	18	1.07 ± 0.02	28
0.99	1.43 ± 0.05	−2.9 ± 0.3	23	1.08 ± 0.02	25

changes in the depth of Hδ may be more visible in absorption systems, indicating that the spectral rotation is driven by the more recent star formation history.

In order to throw more light on this issue, we fitted simple stellar population (SSP) models to our composite spectra. We applied a modified version of the spectral population synthesis code, *starlight* (http://www.starlight.ufsc.br/) [15, 16] to fit the observed and combined spectra. The code does a search for the best-fitting linear combination of 45 simple stellar populations (SSPs), 15 ages, and 3 metallicities (0.2 $Z_\odot$, 1 $Z_\odot$, 2.5 $Z_\odot$) provided by [17] to match a given observed spectrum O_λ. The model spectrum M_λ is

$$M_\lambda(x, M_{\lambda_0}, A_V, \nu_\star, \sigma_\star) = M_{\lambda_0}\left[\sum_{j=1}^{N_\star} x_j b_{j,\lambda} r_\lambda\right] \otimes G(\nu_\star, \sigma_\star), \quad (1)$$

where $b_{j,\lambda} = L_\lambda^{\mathrm{SSP}}(t_j, Z_j)/L_{\lambda_0}^{\mathrm{SSP}}(t_j, Z_j)$ is the spectrum of the jth SSP normalized at λ_0, $r_\lambda = 10^{-0.4(A_\lambda - A_{\lambda_0})}$ is the reddening term, x is the population vector, M_{λ_0} is the synthetic flux at the normalization wavelength, and $G(\nu_\star, \sigma_\star)$ is the line-of-sight stellar velocity distribution modeled as a Gaussian centered at velocity $\nu_\star$ and broadened by $\sigma_\star$. The match between model and observed spectra is calculated as $\chi^2(x, M_{\lambda_0}, A_V, \nu_\star, \sigma_\star) = \sum_{\lambda=1}^{N_\lambda}[(O_\lambda - M_\lambda)w_\lambda]^2$, where the weight spectrum w_λ is defined as the inverse of the noise in O_λ. For more details we refer to the paper by [18]. We rebin the 45 SSPs into 5 components according to age as follows: I ($10^6 \leqslant t < 10^8$ yr), II ($10^8 \leqslant t < 5 \times 10^8$ yr), III ($5 \times 10^8 \leqslant t < 10^9$ yr), IV ($10^9 \leqslant t < 2.5 \times 10^9$ yr), and V ($t \geqslant 2.5 \times 10^9$ yr).

Figure 4 shows an example of the fit for the averaged spectrum at $\langle z \rangle = 0.29$. Panels (a), (b), and (c) correspond to absorption line, emission-line, and all spectra, respectively.

The results summarized in Table 4 clearly show that the fraction of young stars in emission-line spectra and that of intermediate age in absorption systems increase with z.

4. Absorption Line Systems

The spectral resolution of the 300V grism allows us to detect [OII] emission down to EQW([OII]) ∼ 2-3 Å. We will call absorption line galaxies those for which star formation is low enough to preclude [OII] detection at our detection level. Thus, our absorption line sample comprises mostly E, E+A, and S0 galaxies with no ongoing star formation.

4.1. Absorption Systems as Function of Redshift. The normalized and combined spectra of absorption line systems

Table 4: Stellar population properties of normalized average full sample (absorption + emission), absorption (abs), emission (em) spectra in each redshift bin. The magnitude cutoff is at $M_R = -18.8$, except for the 10 faintest absorption systems at $z = 0.29$ where we used all the observed objects.

$\langle z \rangle$	log(Age)	<8	8–8.7	8.7–9	9–9.4	>9.4
0.29	abs	0.0%	0.0%	30.1%	0.1%	69.8%
	abs (10 brightest)	0	0	17.4	0	82.4
	abs (10 faintest)	0	0	12.0	66.4	21.7
	em	16.0	44.1	12.8	1.5	25.7
0.43	abs	0.0	0.7	11.7	6.9	80.7
	em	28.3	14.2	16.5	36.8	4.2
0.65	abs	0.0	0.0	18.2	38.5	43.3
	em	33.1	0.3	65.1	1.4	0.0
0.82	abs	0.0	0.0	86.8	3.3	9.8
	em	21.9	37.1	26.9	0.1	14.1
0.99	abs	0.0	0.0	42.3	0.0	57.7
	em	53.9	9.6	22.7	13.8	0.0

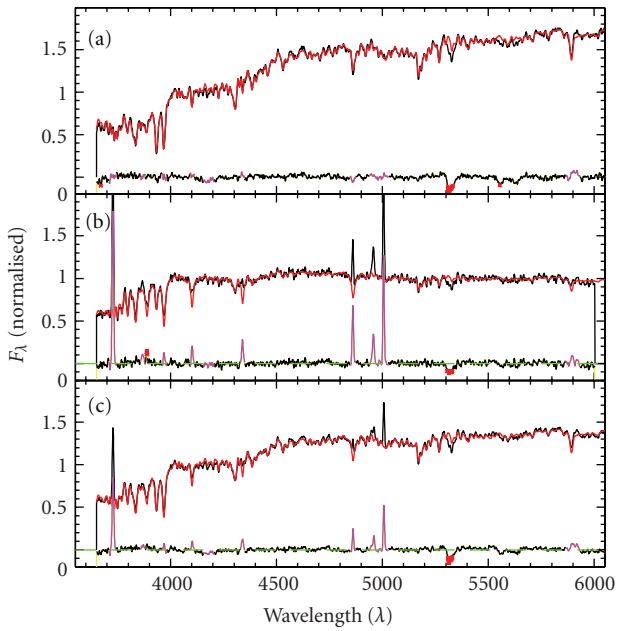

Figure 4: Spectral fitting results with SSP models for the redshift $\langle z \rangle = 0.29$ bin. (a) Observed (thin black line) model (red line) and residuals for the absorption spectrum. Points indicate bad pixels and emission-line windows that were masked out during fitting. (b) Emission-line spectrum; (c) Total spectrum. SSPs do not model emission-lines.

presented in Figure 3(a) have S/N ratios in the range 18–24. They are obtained with spectra of galaxies brighter than $M_R = -18.8$. They do not show any obvious change in their continuum and their 4000 Å break amplitude up to $z \approx 0.6$ (Table 3). There is a small decrease in the 4000 Å break at $z \geqslant 0.65$ ranging from 5% at $z \sim 0.65$ to 15% at $z \sim 1$ while the Hδ absorption line becomes stronger at $z \geqslant 0.65$ (Table 3) suggesting the presence of increasing numbers of A stars at higher redshifts. The indexes suggest that these galaxies had the bulk of their star formation at $z \geqslant 1$, while some of the systems at $z > 0.8$ still had clearly detectable star formation about 1 Gyr ago.

We have compared our spectral indexes at $z \sim 0.82$ with those measured by [19] in the rich cluster MS 1054-03 at $z = 0.83$ using the same index definitions from [13]. The average break amplitude and Hδ index of absorption systems in MS 1054-03 are, respectively, D(4000)(abs) $= 1.67 \pm 0.00$ and EQW(Hδ)(abs) $= -1.7 \pm 0.0$ [19, Table 4]; amplitude of measurement errors estimated by Tran et al. by Monte Carlo. Our absorption systems at $z \sim 0.82$ appear to have younger stellar populations as indicated both by D(4000) and EQW(Hδ) (Table 3). They have clearly less A stars than composite E+A field galaxies at $\langle z \rangle = 0.6$, for which D(4000) (abs) $= 1.36 \pm 0.02$ and EQW(Hδ) (abs) $= -4.6 \pm 0.2$ as measured by Tran et al. [20].

Our SSP models (Table 4) indicate that absorption line systems at $z \geqslant 0.65$ show more than 50% of stars younger than 2.5 Gyrs, while those at $z \geqslant 0.8$ had star formation only about one Gyr ago.

4.2. Absorption Systems as Function of Luminosity at $z = 0.29$. Having tested bright absorption systems at various z (with cutoff at $M_R = -18.8$) we now turn to faint absorption galaxies in the cluster at $\langle z \rangle = 0.29$ by combining the spectra of the 10 faintest galaxies without emission-lines. Their average R-band magnitude is $R = 22$, which at a distance modulus of 40.18 corresponds to $M_R = -18.2$, and the faintest object has $M_R = -17.44$. Their mean indexes, D(4000) $= 1.55 \pm 0.01$; Hδ $= -2.27 \pm 0.04$, measured on the spectrum shown in Figure 5 are consistent with a younger age than absorption line galaxies with $M_R \leqslant -18.8$ (Table 3) in the same cluster. This is in agreement with the well known evidence that the stellar populations in absorption systems tend to be younger in low-mass galaxies than in the more massive ones (e.g., [21]). The index values are in fact very close to those of our bright absorption systems at $z = 0.8$.

Table 5: D(4000), [OII] equivalent width, and $H\delta$ index for emission-line galaxies. Index errors are measured on combined spectra. The number of objects in each bin, N_{gal} is listed in the second column and the rms dispersions in the index distributions within each bin are listed in parenthesis. The values of EQW(Hδ) marked (*) were measured after fitting an underlying absorption profile on spectra displaying Hδ both in absorption and in emission. The S/N ratios of the continuum spectra in the range 4150–4250 Å for a pixel element of 2.6 Å, are given in the last column.

$\langle z \rangle$	$N_{\rm gal}$	D(4000), (σ)	EQW([OII]), (σ)	EQW(Hδ)	*S/N*
0.29	25	1.22 ± 0.02 (0.16)	19.6 ± 0.3 (17)	−3.07 ± 0.2	32
⟨0.43⟩	75	1.22 ± 0.01 (0.14)	17.9 ± 0.3 (12)	−3.01 ± 0.1	52
⟨0.65⟩	60	1.14 ± 0.01 (0.12)	19.0 ± 0.3 (12)	−3.3 ± 0.1	35
0.82	22	1.07 ± 0.02 (0.09)	37.2 ± 0.7 (16)	−5 ± 0.7 (*)	28
⟨0.9⟩	44	1.08 ± 0.01 (0.10)	39.7 ± 0.5 (20)	−5 ± 0.5 (*)	31
0.99	16	1.08 ± 0.02 (0.13)	43.5 ± 0.9 (23)	−5.5 ± 0.7 (*)	25

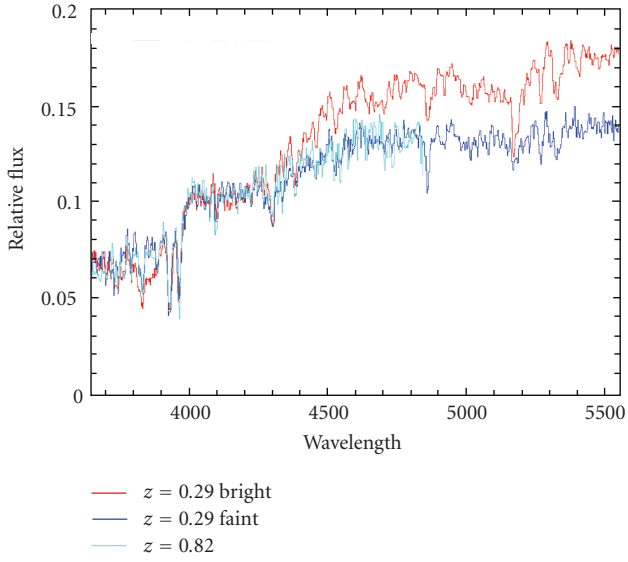

Figure 5: Normalized spectra of the 10 brightest (in red) and the 10 faintest (in blue) absorption-line galaxies in the cluster at $z = 0.29$, and the full sample of absorption-line systems at $z = 0.82$ (in cyan).

The SSP models indicate that on average about 80% of the stars in the 10 faintest galaxies are younger than 2.5 Gyr (Table 4), that is, were born at $z < 1$. For comparison, 80% of the stars contributing to the spectrum of the brightest absorption galaxies in the cluster are older than 2.5 Gyr (Table 4).

To illustrate the full spectrum continuum difference between bright and faint systems at $z = 0.29$ and the similarity of faint spectra at $z = 0.29$ with bright spectra at $z = 0.8$, we have plotted in Figure 5 the average spectra of the 10 brightest and the 10 faintest absorption systems at $z = 0.29$, and the average spectrum at $z = 0.82$.

At a redshift of $z \sim 0.8$ (i.e., ∼4 Gy earlier), the red-sequence of our unrelaxed cluster at $z = 0.29$ (merging central system; elongated intracluster light and galaxy distribution) was already in place but was truncated at brighter magnitudes because those faint absorption systems which have 78% of stars younger than 2.5 Gyr, were in the process of star formation, and would be classified star-forming galaxies. This is consistent with the observation that some clusters at $z \simeq 1$ have red sequences truncated at faint limits [6, 14], and supports the picture of an environmental dependence of red sequence truncation presented by [22]. Our findings are also in agreement with [23] scenarios in which final assembling in the red-sequence can be observed well below $z = 1$. The red sequence at $\langle z \rangle = 0.29$ will be studied in more detail together with the cluster dynamics and the ICL of the RX J0054.0-2823 cluster core in a forthcoming paper [24].

5. Emission-Line Galaxies

After removing the absorption line galaxies from the sample, the variation of the spectral continuum of galaxies with emission-lines as function of redshift becomes significantly stronger (Figure 3(b)). Table 5 gives the values of the physical distribution dispersions $\sigma(D(4000))$ and $\sigma(\mathrm{EQW}([\mathrm{OII}]))$, measured on individual galaxies in each redshift bin.

The observed changes in spectral continuum shape in the local indexes given in Table 5, and in the best fit stellar population models presented in Table 4 take place over cosmological time scales of order 4 Gyr. Since for single bursts the models predict such variations on time scales of less than 2 Gyr, we interpret the observed spectral changes as an evolutionary sequence where, on average, galaxies with various bursts at various rates and ages, "migrate" towards redder types as they evolve. These results are in agreement with the well known steep increase in SFR between redshifts 0 and 1 [25–28].

Before examining this evolution in more detail, we would like to know which fraction of our emission-line objects are AGNs, and which fraction are star-forming galaxies. Methods based upon intensity ratios of emission-lines were devised long ago to distinguish photo-ionization by AGN from star formation [29–31]. Kauffmann et al. [13, 31] isolate star-forming galaxies by using a diagram based upon [OIII]/Hβ and [NII]/Hα which cannot be used here. Nevertheless the condition [OIII]/H$\beta \geqslant 3$ separates well AGNs from star-forming galaxies and LINERs, as shown in Figure 7 of Yan et al. [32]. In order to estimate the AGN contribution we apply the condition [OIII]/H$\beta \geqslant 3$ to the redshift limited region $0.35 \leqslant z \leqslant 0.65$ excluding the cluster at $z = 0.29$. In the layer $\langle z \rangle = 0.68$ the fraction of spectra

Table 6: Values of the 4000 Å break amplitudes and EQW([OII]) dividing "blue" and "red" emission-line galaxies.

$\langle z \rangle$	D(4000)	EQW([OII])
0.29	1.19	19
$\langle 0.43 \rangle$	1.22	18
$\langle 0.65 \rangle$	1.14	19
$\langle 0.9 \rangle$	1.07	37

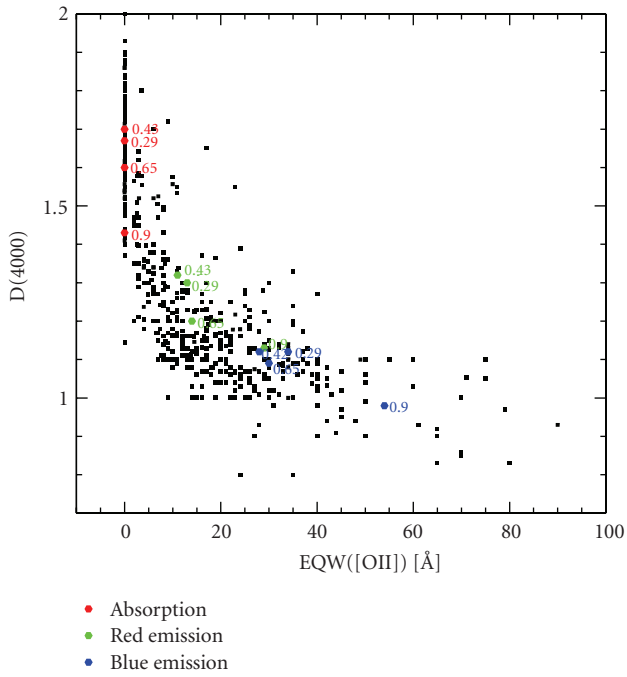

Figure 6: Diagram of the 4000 Å break amplitude plotted versus the equivalent width of [OII] for all the galaxies of our sample. The global parameters measured in the combined spectra are overplotted in different colors labeled by their redshifts. Individual errors are not shown; the bulk of individual spectra have typical errors of 8% in D(4000) and 20% in EQW([OII]).

truncated at $\lambda = 4950$ Å is 16% and increases with z. We find that 8% of our emission-line galaxies have Seyfert spectra.

5.1. Partitioning the Emission-Line Galaxies in "Red" and "Blue" Systems by Their Continuum Slope. In order to examine the evolution of our emission-line galaxies, we partition the sample in two halves: those with continuum slopes bluer than the average and those with continuum slopes redder than the average. Our intention is to divide the data in two groups by using the simplest possible statistical method, with the first group containing starburst galaxies and the second objects in a more advanced evolutionary stage. The resulting values of D(4000) and EQW([OII]) parameters for galaxies with spectral continua near the median of the partition, are given in Table 6.

While a median partition does not necessarily represent a physical partition, in our case the choice is justified by the relation between EQW([OII]) and D(4000) shown in Figure 6.

The average values of EQW([OII]) and D(4000) for "red" and "blue" continuum spectra are overplotted, showing that our *simple* median partition in continuum separates objects with a large spread in D(4000) and small spread in EQW([OII]) (EQW[OII]< 15 Å), from objects with a large spread in EQW([OII]) and small spread in D(4000) ($0.8 <$ D(4000) $\leqslant 1.2$); it divides "young" galaxies, for which the evolution is dominated by ongoing star formation from "old" galaxies where the evolution is dominated by changes in the older stellar populations.

5.2. Blue Emission-Line Galaxies. The average parameters D(4000), EQW([OII]), and EQW(Hδ) of the spectra obtained by combining the blue half of emission systems shown in Figure 7(a) are given in Table 7, and their locations in the (EQW([OII]-D(4000)) diagram are overplotted in Figure 6 as indicated in the caption.

We clearly see in Figure 7(a) that the spectra in the redshift bins $z = 0.29$, 0.43 and 0.65 are basically indistinguishable from each other: they correspond to starbursts showing strong [OII] and bright UV.

The population of Seyferts being small, the spectra of most of blue objects are dominated by an ongoing stellar burst essentially undiluted by older stellar populations. Galaxies with a few giant HII regions diluted by a sufficiently large population of old stars will by definition be part of the red half of the sample. The three redshift bins are separated by ~1 Gyr each in cosmic time, so the starbursts that we are observing in one bin will not be classified as starburst in the next (lower z) bin. Therefore, the population of starburst galaxies must be *repopulated* from one bin to the next either by new star formation events in the same galaxies, or by new galaxies going through the starburst phase. This significant production of new starbursts will populate the starting point of new evolutionary sequences at each redshift. Figure 7(a) also shows that at $z > 0.68$ the blue emission-line galaxies are even bluer than at lower z implying an even higher birthrate of starbursts in the corresponding redshift range $0.8 \leqslant z \leqslant 1$, or a higher nuclear activity. This implies that the populations of starburst galaxies must be continuously repopulated between $z \sim 1$ and $z \sim 0.3$.

5.3. Red Emission-Line Galaxies. After having isolated the two extremes of our galaxy population: starburst dominated emission-line galaxies, and absorption line systems, we now turn to the galaxies in intermediate evolutionary stages.

The middle panel of Figure 7 shows the spectra of the red half of emission-lines galaxies in the corresponding redshift bins. The most conspicuous changes in the spectra are the systematic increase in UV continuum and [OII] strength with redshift. The average values of EQW([OII]), D(4000), and EQW(Hδ) in each redshift bin are given in Table 8 and are overplotted on the (EQW([OII])-D(4000)) diagram of Figure 6 showing an increase by a factor almost 3 in EQW([OII]) between $\langle z \rangle = 0.43$ and $\langle z \rangle = 0.9$ coupled to a significant decline in the amplitude of the 4000 Å break.

In order to quantify the evolution of the continuum to the red of the G band, we introduce a G-step index as the

Table 7: D(4000) and equivalent widths of [OII] and Hδ of average "blue" emission-line galaxies. Values marked (*) have Hδ both in absorption and in emission. In those cases, EQW(Hδ) was measured by fitting a profile to remove the emission component. Objects for which $H\delta$ was not visible in emission (in the $\langle z\rangle = 0.43$ bin) may still have the bottom of the absorption profile contaminated with emission. The S/N ratios of the continuum in the wavelength range 4150–4250 Å are given in the last column.

$\langle z\rangle$	D(4000)	EQW([OII])	EQW(Hδ)	S/N
0.29	1.11 ± 0.01	34.3 ± 0.5	-4 ± 0.5 (*)	23
0.415	1.09 ± 0.01	32.3 ± 0.5	-2.64 ± 0.08	40
$\langle 0.43\rangle$	1.12 ± 0.01	27.9 ± 0.4	-2.84 ± 0.08	49
0.447	1.18 ± 0.01	22.3 ± 0.6	-3.60 ± 0.07	42
0.63	1.07 ± 0.015	40.8 ± 0.7	-3.5 ± 1 (*)	15
$\langle 0.65\rangle$	1.09 ± 0.01	30.3 ± 0.7	-5 ± 0.5 (*)	28
0.68	1.11 ± 0.015	21.3 ± 0.8	-5 ± 0.5 (*)	32
0.82	1.04 ± 0.02	53.1 ± 0.8	-6 ± 0.5 (*)	18
$\langle 0.9\rangle$	1.02 ± 0.015	53.8 ± 0.8	-5.5 ± 0.5 (*)	23
0.99	1.02 ± 0.02	58.8 ± 0.9	-5 ± 0.5 (*)	12

ratio of the [4550–4650] Å to the [4150–4250] Å fluxes. The resulting values are given in Table 8. There is an increase of 16% in the G-step index between $\langle z\rangle = 0.65$ and $\langle z\rangle = 0.29$ and a corresponding increase of 9% in the D(4000) break. These variations reach, respectively, 26% and 15% over the redshift range $\langle z\rangle = 0.9$ to $\langle z\rangle = 0.29$. The G-step of absorption systems, also given in Table 8 for comparison, is in all cases larger than the values for the red emission-line galaxies. The red half of emission-line galaxies must have huge HII regions at $z > 0.6$, while at lower z the HII regions are more diluted by an older stellar continuum similar to what is observed in local early-type spiral galaxies. As noted above, the SSP models show that the single bursts require a much shorter time to reach the red emission-line phase than the time span corresponding to the redshift interval $0.3 < z < 0.6$ ($\sim$2 Gyr). Therefore, we are observing a mix of objects where evolved emission-line galaxies tend to accumulate at lower z.

We have fitted the average spectra of red emission-line galaxies in Figure 7(b) with spectral synthesis population models. The resulting SSPs rebinned into 5 age ranges are given in Table 9. The SSPs clearly show that star formation in red emission-line galaxies is fading at $z < 0.5$ and most of the stars in the observed spectra at $z > 0.5$ are younger than 2.5 Gyr.

5.4. Down-Sizing of Star Formation. The values of the parameters D(40000) and EQW([OII]) that we find in the average *red* spectrum at $\langle z\rangle = 0.9$ (Table 8) are close to those measured on the average *blue* spectra at $z = 0.29$ and $\langle z\rangle = 0.43$ (Table 7), which are also fainter (Table 2). To quantify this *downsizing* effect from $z = 0.9$ to $z = 0.4$ we determine the range of luminosities for which galaxies have spectra similar to luminous ($f \geqslant 1$) galaxies at $\langle z\rangle = 0.9$. Figure 8 shows the average spectra of bright and faint red emission systems at $\langle z\rangle = 0.43$. The "faint" objects at $\langle z\rangle = 0.43$ have an average magnitude $R = 21.9$, that is, $M_R = -19.0$ or $f \approx 0.3$ while "bright" objects have $f \approx 1.66$. Best fitting SSP models are overplotted and the corresponding stellar populations are reported in Table 10. Clearly the stellar mix in our red galaxies at $\langle z\rangle = 0.9$ (Table 9) has less young stars than our faint galaxies at $z < 0.5$, and less intermediate-old stars than our bright, $f \geqslant 1$, galaxies at $z < 0.5$. We thus scanned the magnitude range of all our emission-line galaxies at $\langle z\rangle = 0.43$ with a band of magnitude $\Delta m \sim 1-1.5$, averaged the selected spectra, and compared the averages to the spectrum of bright galaxies at $\langle z\rangle = 0.9$. Residuals were calculated after scaling the $\langle z\rangle = 0.43$ spectrum to the same flux at 4150–4250 Å as for the $\langle z\rangle = 0.9$ bright spectrum. The minimum in the residuals was obtained by combining spectra in the magnitude range $21.5 \leqslant R \leqslant 22.4$. The average spectrum at $\langle z\rangle = 0.43$ and the difference with the bright spectrum at $\langle z\rangle = 0.9$ are shown in Figure 9.

The emission-line galaxies which were used to obtain the above spectrum at $\langle z\rangle = 0.43$ have a mean magnitude of $R = -19.86$, or $\langle f\rangle = 0.40 \pm 0.03$ at 4150–4250 Å while the bright emission-line galaxies at $\langle z\rangle = 0.9$ have $\langle f\rangle = 1.6 \pm 0.3$, a factor of 4 larger! Therefore, the downsizing phenomenon in our sample is of 1.2–1.7 magnitudes from $z = 0.9$ to $z = 0.4$.

Clearly there is a population of bright red emission-line galaxies at $z = 0.4$ which we have not at $z = 0.9$. The results of population synthesis models presented in Table 11 indicate that the bright red emission-line galaxies at $z < 0.5$ are the oldest. They are indeed the only ones where we detect significant populations of stars older than 2.5 Gyr. We also find that galaxies with stars older than 2.5 Gyr carry no weight in the $\langle z\rangle = 0.65$ bin. So these objects are rare at $z > 0.5$.

5.5. The Red Limit of Emission-Line Galaxies. At each z we have selected those galaxies with the reddest continuum (the reddest quartile at each redshift bin). We will refer to the combined spectra of these extreme sample as the red envelope or red limit of emission-line galaxies. Since we are working with small numbers of galaxies, typically 5–10, it was necessary to combine the samples at $z = 0.82$ and $z = 0.99$ to improve statistics. Nevertheless, because our red emission-line galaxies are rather luminous the combined continuum spectra still have high S/N ratios (Table 12). The resulting spectra are shown in Figure 7(c). The common

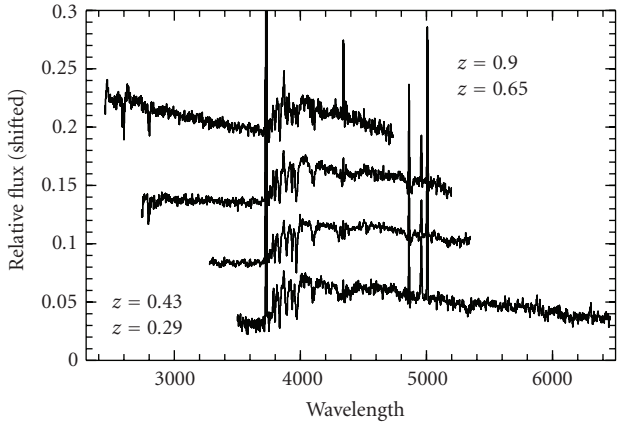

(a)

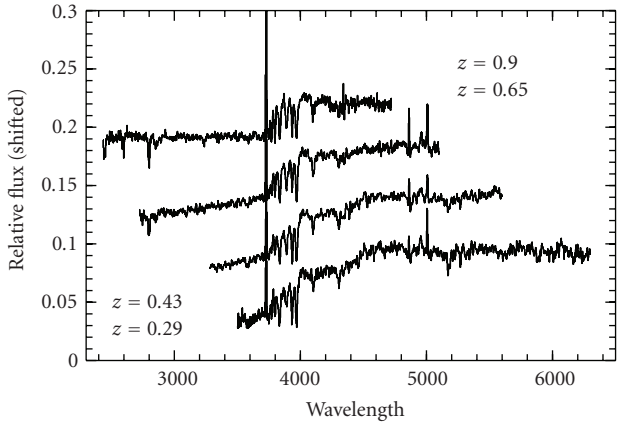

(b)

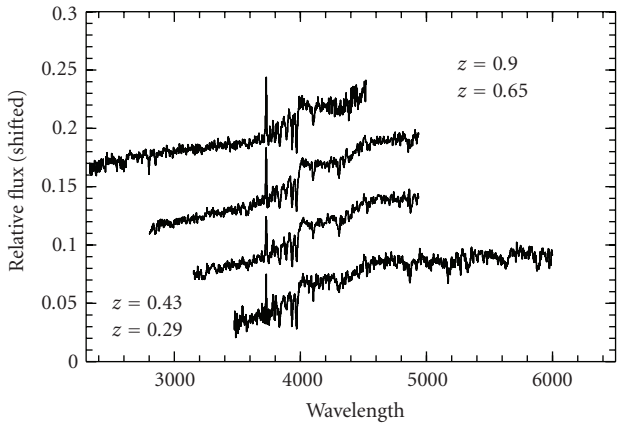

(c)

Figure 7: Composite spectra of galaxies with emission-lines: (a) blue half; (b) red half; and (c) reddest. Spectra have been normalized in the wavelength range $\Delta\lambda = 4050$–4250 Å and shifted for clarity. The S/N ratios of the continuum in the wavelength range 4150–4250 Å are given in Tables 7, 8, and 12.Note the probable contamination of blue spectra by Seyferts (conventionally defined as galaxies with [OIII] $\geqslant 3 \times$ Hβ; [30]).

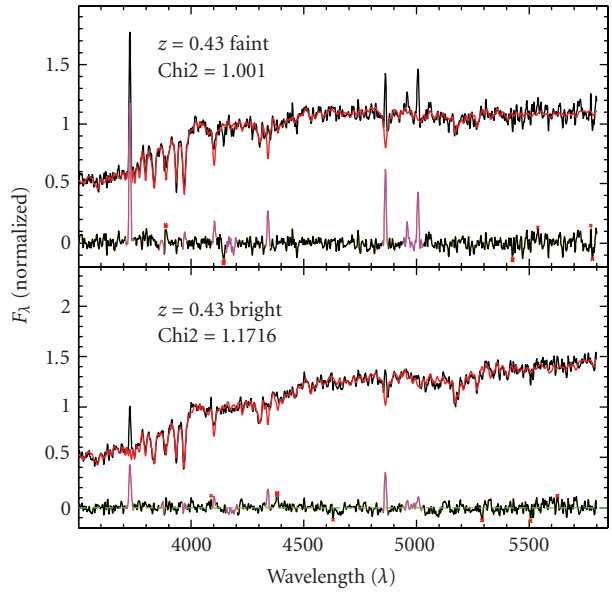

Figure 8: Spectra of faint ($f \approx 0.3$) and bright ($f \approx 1.65$) emission systems in the $\langle z \rangle = 0.43$ redshift bin. SSP models with parameters in Tables 10 and 11 are overplotted.

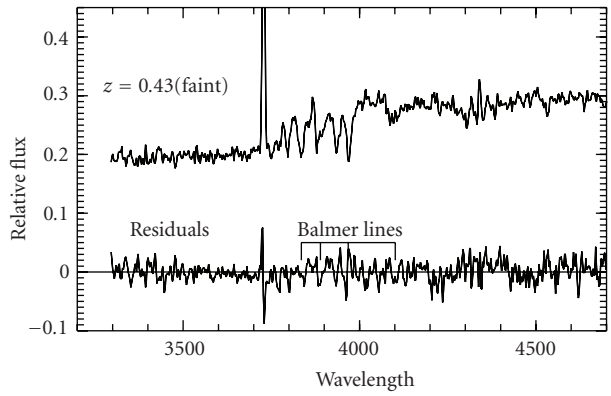

Figure 9: Combined spectrum of emission systems in the $\langle z \rangle = 0.43$ redshift bin selected in the magnitude range $21.5 \leqslant R \leqslant 22.4$ (with $\langle f \rangle = 0.4 \pm 0.03$) and residuals between this spectrum and that of bright (f $\geqslant 1$; $\langle f \rangle = 1.6 \pm 0.3$) emission-line galaxies at $\langle z \rangle = 0.9$.

parts of the red envelopes of spectra at $\langle z \rangle = 0.29$, $\langle z \rangle = 0.43$, $\langle z \rangle = 0.65$ are similar, while the red limit at $\langle z \rangle = 0.9$ has higher UV continuum. Both the continuum and the indexes of the red limit at $z \leqslant 0.68$ (i.e., D(4000) $\sim$ 1.35–1.45, EQW([OII]) $\sim$ 4–8), are typical of nearby spirals with prominent bulges and low star formation [12, 33, 34], or early-type LINERs. Up to $z \sim 0.7$ the populations of red spirals and early-types can be well separated by their morphology. The higher UV continuum and lower D(4000) break amplitude of the limit spectrum at $\langle z \rangle = 0.9$ indicate that such red objects become rare at $z \geqslant 0.68$ in our sample.

5.6. Antihierarchical Galaxy Evolution. There are blue galaxies in each bin that are at least one magnitude brighter

Table 8: Equivalent widths of [OII] and $H\delta$ in absorption, 4000 Å break amplitudes, and G-step indexes for "red" emission systems. The number of galaxies in each bin (N_{gal}) is given in the second column and the rms dispersions EQW([OII]) and D(4000) within each bin are given in parenthesis as in Table 5. The values of $EQW(H\delta)$ marked with a (*) are measured as in Table 7. The S/N continuum ratios are measured as in Table 5. The G-steps of absorption systems are listed in the last column for comparison.

$\langle z \rangle$	N_{gal}	EQW([OII])	D(4000)	EQW(Hδ)	G step	S/N	G step (abs)
0.29	13	13.2 ± 0.3 (11)	1.324 ± 0.038 (0.53)	−1.89 ± 0.05	1.221 ± 0.012	27	1.470 ± 0.018
0.415	22	8.9 ± 0.4 (3.8)	1.330 ± 0.044 (0.17)	−2.34 ± 0.05	1.181 ± 0.015	28	—
⟨0.43⟩	38	10.7 ± 0.5 (4.6)	1.317 ± 0.038 (0.15)	−2.32 ± 0.05	1.164 ± 0.012	34	1.423 ± 0.018
0.447	16	10.5 ± 0.5 (5.5)	1.300 ± 0.040 (0.13)	−2.48 ± 0.07	1.142 ± 0.016	34	—
0.63	17	13.9 ± 0.5 (6.6)	1.182 ± 0.032 (0.12)	−3.80 ± 0.05	1.056 ± 0.014	29	—
⟨0.65⟩	29	14.3 ± 0.5 (6.0)	1.197 ± 0.037 (0.10)	−4.42 ± 0.05	1.054 ± 0.010	37	1.369 ± 0.017
0.68	12	17.0 ± 0.7 (5.8)	1.215 ± 0.040 (0.07)	−5.0 ± 0.1	1.054 ± 0.012	28	—
0.82	11	26.7 ± 0.7 (12.5)	1.118 ± 0.038 (0.08)	−4.6 ± 0.5 (*)	0.977 ± 0.019	22	—
⟨0.9⟩	23	29.5 ± 0.6 (19)	1.132 ± 0.040 (0.09)	−5.3 ± 0.3 (*)	0.971 ± 0.015	25	1.325 ± 0.034
0.99	9	30.3 ± 0.7 (19.7)	1.150 ± 0.050 (0.07)	−5.5 ± 0.5 (*)	0.965 ± 0.020	20	—

Table 9: Stellar population properties of red emission-line galaxies.

$\langle z \rangle$	log Age					χ^2
	<8	8–8.7	8.7–9	9–9.4	>9.4	
0.29	0.0	28.3	16.6	25.5	29.5	1.20
0.43	9.0	20.8	30.8	32.7	6.7	0.70
0.65	13.8	25.1	40.9	20.2	0.0	0.68
0.9	18.0	33.2	15.2	33.6	0.0	0.75

Table 10: Stellar population properties of faint ($f \approx 0.3$) red emission-line galaxies at $z < 0.5$.

$\langle z \rangle$	log Age					χ^2
	<8	8–8.7	8.7–9	9–9.4	>9.4	
0.29 (faint)	37	0	59	0	3.8	2.1
0.43 (faint)	24	6	41	24	4.5	1.0

Table 11: Stellar population properties of red emission-line galaxies with luminosity $f > 1$.

$\langle z \rangle$	log Age					χ^2
	<8	8–8.7	8.7–9	9–9.4	>9.4	
0.29	0.0	22.5	31.6	7.7	38.2	1.50
0.43	19.0	0.1	48.0	0.9	32.0	1.17
0.65	6.2	40.8	24.5	28.5	0.0	1.15

Table 12: Equivalent width of [OII], 4000 Å break amplitude, $H\delta$ index, and the G-step of the red envelope of emission-line galaxies. The continuum S/N ratios are given in the last column.

$\langle z \rangle$	EQW([OII])	D(4000)	EQW(Hδ)	G step	S/N
0.29	4.2 ± 0.3	1.35 ± 0.07	−1.8 ± 0.3	1.224 ± 0.017	19
0.43	8.5 ± 0.2	1.39 ± 0.06	−2.5 ± 0.2	1.268 ± 0.014	24
0.65	8.3 ± 0.2	1.44 ± 0.06	−3.0 ± 0.2	1.273 ± 0.012	29
0.9	9.0 ± 0.3	1.30 ± 0.07	−3.9 ± 0.2	—	18

than the average in their redshift bin, and, consequently, that are brighter than the average of red galaxies in the next (lower z) bin. Therefore, as the starbursts fade, some of the parent galaxies will fall below our magnitude limit and leave the sample, while others will migrate to the red half of the next lower redshift bin. This indicates that the two populations are connected and that the starbursts in one bin will evolve to populate the fainter portion of the distribution of red emission-line galaxies in the next bin at lower redshift. A typical starburst galaxy in one redshift bin, however, is not sufficiently luminous to populate the whole range of luminosities of red emission-line galaxies in the next bin, so the brightest red galaxies must come from older and brighter starbursts.

The fainter emission-line galaxies may have had more recent starbursts than the brighter ones, but also the frequency of starbursts must be decreasing to explain the extension of red spectrum types to fainter objects. The downsizing is, therefore, twofold: in the range $0.3 \leqslant z \leqslant 1$ both the luminosity and the frequency of starbursts decrease with time. It is as if the strongest mode of star formation switches off progressively from the brightest to the faintest systems. The Universe produces smaller and smaller starbursts systems as it evolves: the large become old and small become beautiful.

We are in fact observing a combination of four effects, of which the following three are shifting from bright to faint systems with decreasing z: strong star formation in emission-line galaxies; aging in emission-line galaxies; and aging in absorption systems. The fourth effect is the repopulation of starbursts in each redshift bin.

Cold Dark Matter (CDM) models are hierarchical in the sense that large halos are built from the merging of small halos. Our observations indicate that, similarly to what has been observed for ellipticals in clusters [35], in our pencilbeam sample of the Universe star formation and halo assemblage are not in phase. This would imply that the era when CDM merging and star formation were massively in phase was much further in the past.

The abundance of haloes of various masses forming at a given time is very broad and is not a simple hierarchical model in which large halo form at a late time [36]. The gravitational sequence of halo formation may be further modified by the galaxy formation physics which may change the efficiency of galaxy formation as function of halo mass. Simulations that incorporate a shutdown seem to be able to reproduce downsizing trends [37]. Gravitational shifts in halo formation time are enhanced by the inclusion of AGN feedback [38–40]. It would be important to compare our data with large ΛCDM simulations, such as for example the "Millenium Run" [41] to determine which physical ingredients need to be added to CDM halo buildings to reproduce our observations.

6. Summary and Conclusions

We have analysed spectral energy distributions as function of redshift of a magnitude limited sample up to $z \sim 1$ in a pencil beam survey of $\approx 10' \times 10'$. The redshift range has been divided in bins centered on the structures that were detected in the (RA, Dec, z) pseudovolume. The redshift bins correspond to cosmic time slices of ∼1 Gyr. Our sample of more than 600 galaxies is reasonably well populated for galaxies brighter than $M_R = -18.8$ up to $z \approx 0.5$; at $z \geqslant 0.75$ the cutoff is at -20.5.

For each redshift bin combined the spectra normalized to the same flux in the wavelength range 4050–4250 Å so in the combined spectra each galaxy has equal weight. This allowed us to study the evolution of the *galaxy populations* independently of luminosity, and thus to extract spectral properties going from bright high-z galaxies to fainter low-z objects. We recovered the luminosity information by calibrating the spectra with broad-band photometry. From this analysis we reach the following conclusions:

(i) While absorption line galaxies do not show significant variation in their continuum energy distributions up to $z = 0.6$, we find that those at $z \geqslant 0.8$ still had some star formation about 1 Gyr earlier. Moreover the faint absorption line galaxies in our dynamically young cluster at $z = 0.29$ have indexes similar to those of bright absorption line systems at $z = 0.8$, suggesting that faint galaxies without emission-lines tend to be younger than more massive galaxies with similar spectra. Our population synthesis models indicate that 50% of the stars contributing to the spectra of faint absorption line galaxies at $z = 0.29$ were formed at $z < 1$. This is consistent with cases of truncated red sequences observed in some high-z clusters and suggests that clusters with truncated red-sequences may be dynamically young. This also suggests that the red sequence is still in a building phase at $z \leqslant 1$.

(ii) The average spectra of galaxies with emission-lines show significant systematic variations in their energy distribution with z, consistent with what is observed in other regions of the Universe. However because the original observations were targetted at measuring the intergalactic light in a X-ray emitting cluster, the survey region is not typical, we present results that are still valid when the foreground cluster at $z = 0.29$ is ignored. In our sample the "downsizing" phenomenon is of 1.2–1.7 magnitudes from $z = 0.4$ to $z = 0.9$. When we divide the sample of emission-line galaxies in two halves by continuum color, we find that the spectral variations are consistent with the following scenario:

(a) the brightest red emission-line galaxies at $z < 0.5$ have the oldest stellar populations;

(b) the Universe at $z \leqslant 0.65$ is repopulated with starburst galaxies at a constant rate down to $z \simeq 0.3$ while at $z \geqslant 0.65$ the birthrate of starbursts is higher;

(c) the red half of emission-line galaxies become redder with decreasing redshift and have lower EQW([OII]) and higher D(4000), which we interpret as the migration of a mix of galaxies

of different ages towards galaxies with diluted star formation or low photo-ionization. Red galaxies with diluted star formation would be in a late phase of smooth star formation.

(iii) The red limit in the energy distribution of emission-line galaxies at $z \leqslant 0.6$ is typical of bulge-dominated spiral galaxies with moderate star formation.

(iv) The intrinsic luminosities of starbursts decline with cosmological time, and continue to decrease also in the next evolutionary phase. Therefore, downsizing must take place both in luminosity *and* in number density.

To summarize, we find that as cosmological time increases, star formation occurs predominatly in smaller and smaller halos, implying that star formation and halo assemblage in our pencil beam are not in phase.

Acknowledgments

This work was based on observations obtained in service mode at the European Southern Observatory at Paranal. E. Giraud thanks the hospitality of ESO and Universidad Catolica in Santiago during the initial phase of this work. J. Melnick thanks the hospitality of Nanjing University during the initial phase of this research. Q.-S. Gu would like to acknowledge the financial support from the China Scholarship Council (CSC), the National Natural Science Foundation of China under Grants 10878010, 10221001, and 10633040, and the National Basic Research Program (973 program no. 2007CB815405). H. Quintana thanks partial support from FONDAP "Centro de Astrofísica". P. Zelaya acknowledges a studentship from CONICYT. The authors thank S. di Serego Alighieri for reading a preliminary version of the paper and for his suggestions.

References

[1] J. Melnick, F. Selman, and H. Quintana, "Sky subtraction for deep surface photometry of the intergalactic light from clusters of galaxies," *PASP*, vol. 111, no. 765, pp. 1444–1450, 1999.

[2] M. Dickinson, C. Papovich, H. C. Ferguson, and T. Budavári, "The evolution of the global stellar mass density at $0 < z < 3$," *Astrophysical Journal*, vol. 587, no. 1, pp. 25–40, 2003.

[3] F. Hammer, H. Flores, D. Elbaz, X. Z. Zheng, Y. C. Liang, and C. Cesarsky, "Did most present-day spirals form during the last 8 Gyr? a formation history with violent episodes revealed by panchromatic observations," *Astronomy and Astrophysics*, vol. 430, no. 1, pp. 115–128, 2005.

[4] B. J. Weiner, A. C. Phillips, S. M. Faber et al., "The deep groth strip galaxy redshift survey. III. Redshift catalog and properties of galaxies," *Astrophysical Journal*, vol. 620, no. 2 I, pp. 595–617, 2005.

[5] L. L. Cowie, A. Songaila, E. M. Hu, and J. G. Cohen, "New insight on galaxy formation and evolution from keck spectroscopy of the Hawaii deep fields," *Astronomical Journal*, vol. 112, no. 3, pp. 839–864, 1996.

[6] T. Kodama, T. Yamada, M. Akiyama et al., "Down-sizing in galaxy formation at $z \sim 1$ in the Subaru/*XMM-Newton* deep survey (SXDS)," *Monthly Notices of the Royal Astronomical Society*, vol. 350, no. 3, pp. 1005–1014, 2004.

[7] E. F. Bell, C. Papovich, E. Le Floc'h et al., "Toward an understanding of the rapid decline of the cosmic star formation rate," *Astrophysical Journal*, vol. 625, no. 1 I, pp. 23–36, 2005.

[8] D. Thomas, C. Maraston, R. Bender, and C. M. de Oliveira, "The epochs of early-type galaxy formation as a function of environment," *Astrophysical Journal*, vol. 621, no. 2 I, pp. 673–694, 2005.

[9] M. S. Clemens, A. Bressan, B. Nikolic, P. Alexander, F. Annibali, and R. Rampazzo, "The star formation history of early-type galaxies as a function of mass and environment," *Monthly Notices of the Royal Astronomical Society*, vol. 370, no. 2, pp. 702–720, 2006.

[10] FORS1+2 User Manual VLT-MAN-ESO-13100-1543 Issue 4, 2005.

[11] E. Giraud, Q.-S. Gu, J. Melnick et al., "Low-ionization galaxies and evolution in a pilot survey up to $z = 1$," *Research in Astronomy and Astrophysics*, in press, 2011.

[12] M. L. Balogh, S. L. Morris, H. K. C. Yee, R. G. Carlberg, and E. Ellingson, "Differential galaxy evolution in cluster and field galaxies at $z \approx 0.3$," *Astrophysical Journal*, vol. 527, no. 1, pp. 54–79, 1999.

[13] G. Kauffmann, T. M. Heckman, S. D. M. White et al., "Stellar masses and star formation histories for 105 galaxies from the Sloan Digital Sky Survey," *Monthly Notices of the Royal Astronomical Society*, vol. 341, no. 1, pp. 33–53, 2003.

[14] Y. Koyama, T. Kodama, M. Tanaka, K. Shimasaku, and S. Okamura, "Dependence of the build-up of the colour-magnitude relation on cluster richness at $z \sim 0.8$," *Monthly Notices of the Royal Astronomical Society*, vol. 382, no. 4, pp. 1719–1728, 2007.

[15] R. Cid Fernandes, Q. Gu, J. Melnick et al., "The star formation history of Seyfert 2 nuclei," *Monthly Notices of the Royal Astronomical Society*, vol. 355, no. 1, pp. 273–296, 2004.

[16] Q. Gu, J. Melnick, R. C. Fernandes, D. Kunth, E. Terlevich, and R. Terlevich, "Emission-line properties of Seyfert 2 nuclei," *Monthly Notices of the Royal Astronomical Society*, vol. 366, no. 2, pp. 480–490, 2006.

[17] G. Bruzual and S. Charlot, "Stellar population synthesis at the resolution of 2003," *Monthly Notices of the Royal Astronomical Society*, vol. 344, no. 4, pp. 1000–1028, 2003.

[18] R. Cid Fernandas, A. Mateus, L. Sodré Jr., G. Stasińska, and J. M. Gomes, "Semi-empirical analysis of Sloan Digital Sky Survey galaxies -I. Spectral synthesis method," *Monthly Notices of the Royal Astronomical Society*, vol. 358, no. 2, pp. 363–378, 2005.

[19] K.-V. H. Tran, M. Franx, G. D. Illingworth et al., "A keck spectroscopic survey of MS 1054-03 (z = 0.83): Forming the red sequence," *Astrophysical Journal*, vol. 661, no. 2, pp. 750–767, 2007.

[20] K.-V. H. Tran, M. Franx, G. D. Illingworth, P. Van Dokkum, D. D. Kelson, and D. Daniel Magee, "Field E+A galaxies at intermediate redshifts ($0.3 < z < 1$)," *Astrophysical Journal*, vol. 609, no. 2, pp. 683–691, 2004.

[21] A. Renzini, "Stellar population diagnostics of elliptical galaxy formation," *Annual Review of Astronomy and Astrophysics*, vol. 44, pp. 141–192, 2006.

[22] M. Tanaka, T. Kodama, N. Arimoto et al., "The build-up of the colour-magnitude relation as a function of environment," *Monthly Notices of the Royal Astronomical Society*, vol. 362, no. 1, pp. 268–288, 2005.

[23] S. M. Faber, C. N. A. Willmer, C. Wolf et al., "Galaxy luminosity functions to $z \sim 1$ from DEEP2 and COMBO-17:

implications for red galaxy formation," *Astrophysical Journal*, vol. 665, no. 1, pp. 265–294, 2007.

[24] I. Toledo, F. Selman, E. Giraud, J. Melnick, and H. Quintana, "Diffuse Intracluster Light at Intermediate Redshifts: ICL observations in the X-ray cluster RXJ0054-2823 at $z = 0.29$," in preparation.

[25] Y. C. Pei and S. M. Fall, "Cosmic chemical evolution," *Astrophysical Journal*, vol. 454, no. 1, pp. 69–76, 1995.

[26] S. J. Lilly, O. Le Fèvre, F. Hammer, and D. Crampton, "The canada-france redshift survey: the luminosity density and star formation history of the universe to $z \sim 1$," *Astrophysical Journal*, vol. 460, no. 1, pp. L1–L4, 1996.

[27] P. Madau, L. Pozzetti, and M. Dickinson, "The star formation history of field galaxies," *Astrophysical Journal*, vol. 498, no. 1, pp. 106–116, 1998.

[28] A. M. Hopkins and J. F. Beacom, "On the normalization of the cosmic star formation history," *Astrophysical Journal*, vol. 651, no. 1 I, pp. 142–154, 2006.

[29] J. A. Baldwin, M. M. Phillips, and R. Terlevitch, "Classification parameters for the emission-line spectra of extragalactic objects," *PASP*, vol. 93, p. 5, 1981.

[30] S. Veilleux and D. E. Osterbrock, "Spectral classification of emission-line galaxies," *Astrophysical Journal Supplement Series*, vol. 63, pp. 295–310, 1987.

[31] G. Kauffmann, T. M. Heckman, C. Tremonti et al., "The host galaxies of active galactic nuclei," *Monthly Notices of the Royal Astronomical Society*, vol. 346, no. 4, pp. 1055–1077, 2003.

[32] R. Yan, J. A. Newman, S. M. Faber, N. Konidaris, D. Koo, and M. Davis, "On the origin of [O II] emission in red-sequence and poststarburst galaxies," *Astrophysical Journal*, vol. 648, no. 1, pp. 281–298, 2006.

[33] R. C. Kennicutt Jr., "A spectrophotometric atlas of galaxies," *Astrophysical Journal, Supplement Series*, vol. 79, no. 2, pp. 255–284, 1992.

[34] A. L. Kinney, D. Calzetti, R. C. Bohlin, K. Mcquade, T. Storchi-Bergmann, and H. R. Schmitt, "Template ultraviolet to near-infrared spectra of star-forming galaxies and their application to K-corrections," *Astrophysical Journal*, vol. 467, no. 1, pp. 38–60, 1996.

[35] C. M. Baugh, S. Cole, and C. S. Frenk, "Evolution of the Bubble sequence in hierarchical models for galaxy formation," *Monthly Notices of the Royal Astronomical Society*, vol. 283, no. 4, pp. 1361–1378, 1996.

[36] H. J. Mo and S. D. M. White, "The abundance and clustering of dark haloes in the standard ΛCDM cosmogony," *Monthly Notices of the Royal Astronomical Society*, vol. 336, no. 1, pp. 112–118, 2002.

[37] A. Cattaneo, A. Dekel, S. M. Faber, and B. Guiderdoni, "Downsizing by shutdown in red galaxies," *Monthly Notices of the Royal Astronomical Society*, vol. 389, no. 2, pp. 567–584, 2008.

[38] R. G. Bower, A. J. Benson, R. Malbon et al., "Breaking the hierarchy of galaxy formation," *Monthly Notices of the Royal Astronomical Society*, vol. 370, no. 2, pp. 645–655, 2006.

[39] D. J. Croton, V. Springel, S. D. M. White et al., "The many lives of active galactic nuclei: cooling flows, black holes and the luminosities and colours of galaxies," *Monthly Notices of the Royal Astronomical Society*, vol. 365, no. 1, pp. 11–28, 2006.

[40] C. D. P. Lagos, S. A. Cora, and N. D. Padilla, "Effects of AGN feedback on ΛcDM galaxies," *Monthly Notices of the Royal Astronomical Society*, vol. 388, no. 2, pp. 587–602, 2008.

[41] V. Springel, S. D. M. White, A. Jenkins et al., "Simulations of the formation, evolution and clustering of galaxies and quasars," *Nature*, vol. 435, no. 7042, pp. 629–636, 2005.